Yang et al. World Allergy Organization Journal (2024) 17:100964
http://doi.org/10.1016/j.waojou.2024.100964

WORLD ALLERGY ORGANIZATION JOURNAL

Open Access

Integrated machine learning and bioinformatic analysis of mitochondrial-related signature in chronic rhinosinusitis with nasal polyps

Bo Yang, MMed[a], Min Gu, MMed[a], Chen Hong, MMed[a], Xin-Yuan Zou, MMed[a,1], Jia-Qi Zhang, MBBS[a], Ye Yuan, MBBS[a], Chang-Yu Qiu, MD, MSc[a,b], Mei-Ping Lu, MD, PhD[a]** and Lei Cheng, MD, PhD[a,b]*

ABSTRACT

Background: Chronic rhinosinusitis with nasal polyps (CRSwNP) is a prevalent inflammatory disorder affecting the upper respiratory tract. Recent studies have indicated an association between CRSwNP and mitochondrial metabolic disorder characterized by impaired metabolic pathways; however, the precise mechanisms remain unclear. This study aims to investigate the mitochondrial-related signature in individuals diagnosed with CRSwNP.

Methods: Through the integration of differentially expressed genes (DEGs) with the mitochondrial gene set, differentially expressed mitochondrial-related genes (DEMRGs) were identified. Subsequently, the hub DEMRGs were selected using 4 integrated machine learning algorithms. Immune and mitochondrial characteristics were estimated based on CIBERSORT and ssGSEA algorithms. Bioinformatic findings were confirmed through RT-qPCR, immunohistochemistry, and ELISA for nasal tissues, as well as Western blotting analysis for human nasal epithelial cells (hNECs). The relationship between hub DEMRGs and disease severity was assessed using Spearman correlation analysis.

Results: A total of 24 DEMRGs were screened, most of which exhibited lower expression levels in CRSwNP samples. Five hub DEMRGs (*ALDH1L1*, *BCKDHB*, *CBR3*, *HMGCS2*, and *OXR1*) were consistently downregulated in both the discovery and validation cohorts. The hub genes showed a high diagnostic performance and were positively correlated with the infiltration of M2 macrophages and resting mast cells. Experimental results confirmed that the 5 genes were downregulated at both the mRNA and protein levels within nasal polyp tissues. Finally, a significant and inverse relationship was identified between the expression levels of these genes and both the Lund-Mackay and Lund-Kennedy scores.

[a]Department of Otorhinolaryngology & Clinical Allergy Center, The First Affiliated Hospital, Nanjing Medical University, Nanjing, China
*Corresponding author. Department of Otorhinolaryngology & Clinical Allergy Center, The First Affiliated Hospital, Nanjing Medical University, 300 Guangzhou Road, Nanjing 210029, China. E-mail: chenglei@jsph.org.cn
**Corresponding author. Department of Otorhinolaryngology & Clinical Allergy Center, The First Affiliated Hospital, Nanjing Medical University, 300 Guangzhou Road, Nanjing 210029, China. Email: lmp@njmu.edu.cn
[1] Present address: Department of Otorhinolaryngology, The Fourth Affiliated Hospital, Nanjing Medical University, Nanjing, China.

Full list of author information is available at the end of the article

http://doi.org/10.1016/j.waojou.2024.100964
Received 20 January 2024; Received in revised from 31 July 2024; Accepted 11 August 2024
Online publication date xxx

Conclusion: Our findings systematically unraveled 5 hub markers correlated with mitochondrial metabolism and immune cell infiltration in CRSwNP, suggesting their potential to be based to design diagnostic and therapeutic strategies for the disease.

Keywords: Computational biology, Machine learning, Mitochondria, Nasal polyps, Rhinosinusitis

INTRODUCTION

Chronic rhinosinusitis with nasal polyps (CRSwNP) is a prevalent inflammatory disorder in the upper respiratory tract.[1] Compared to chronic rhinosinusitis without nasal polyps (CRSsNP), CRSwNP is typically manifested with more severe clinical symptoms, concurrent with a higher likelihood of asthma, and accompanied with more recurrences after endoscopic sinus surgery.[2] Numerous studies have aimed to elucidate the mechanisms of CRSwNP, yet its precise etiology and pathophysiology remain unclear. It is imperative to identify reliable biomarkers forecasting the onset and progression of the disease.

Mitochondria assist in energy production through oxidative phosphorylation (OXPHOS), resulting in the synthesis of adenosine triphosphate (ATP).[3] Recent evidence indicates that mitochondria intricately regulate various cellular processes, including mitophagy, cellular growth, and the generation of reactive oxygen species (ROS) triggered by inflammation and stress signaling.[4] As a chronic inflammatory disease in the upper airway, CRSwNP is aggravated by mitochondrial dysfunction and ROS overproduction.[5] Epithelial cells originating from nasal polyps exhibit mitochondrial dysfunction in response to environmental contaminants, allergens, and pathogens, leading to the release of a range of proinflammatory cytokines.[6] Compared to normal epithelium, the markers of mitochondrial fusion and fission, as well as mitophagy, are elevated in the epithelium of nasal polyps.[7] These findings suggest that mitochondria play a crucial role in the pathogenesis of CRSwNP and present a potential therapeutic target for intervention.

CRSwNP can be categorized into 3 inflammatory endotypes based on the patterns of immune cell infiltration: type 1, type 2, and type 3.[8] Type 2 CRSwNP is distinguished by significant eosinophilic infiltration, correlating with increased allergic symptoms and a poorer prognosis. Mitochondrial metabolism disorder contributes to the progression of allergic diseases through altering the immune microenvironment.[9] In experimental models of allergic rhinitis, mice with pre-existing deficiencies in mitochondrial electron transport chain exhibit heightened IgE responses, significant airway remodeling and hyperresponsiveness.[10] In asthma, type 2 cytokine IL-4 modulates asymmetric dimethylarginine (ADMA) metabolism, leading to a reduction in mitochondrial quantity and an increase in mitochondrial ROS, thus exacerbating damage to the airway epithelium.[11] Though a growing body of evidence suggests a potential link between immunity and mitochondrial function in CRSwNP, the modulatory effects of mitochondrial-related genes on type 2 inflammation remain to be explored.

Bioinformatics enables the identification of molecules that exhibit differential expression between diseased and healthy individuals. Employing this approach, the current study examined the influence of mitochondrial-related genes on the progression of CRSwNP and their correlation with immune infiltration. In addition, this study explored the correlation between the expression of these hub genes and the severity of CRSwNP, facilitating the development of personalized treatment strategies.

MATERIALS AND METHODS

Gene expression profiles

Datasets GSE136825,[12] GSE36830,[13] and GSE23552[14] were procured from the Gene Expression Omnibus (GEO) database. A total of 42 nasal polyp tissues and 28 control samples were selected from GSE136825, and 6 nasal

polyp tissues along with 6 control samples were chosen from GSE36830. Both datasets were combined to create the discovery set. Furthermore, 11 nasal polyp tissues and 13 control samples from GSE23552 were used for validation. For analysis at single-cell levels, we obtained scRNA-seq dataset SCP253[15] from the Single Cell Portal, including 6 nasal polyp samples and 6 control samples. Supplementary Table 1 provides the information regarding the specifics of each dataset.

Screening of differentially expressed genes (DEGs)

The R package "sva" was utilized to combine the datasets GSE136825 and GSE36830, with batch information excluded. Following this, the R package "limma" was employed to screen the differentially expressed genes (DEGs) between nasal polyps and normal nasal mucosa. In order to visually depict the differential gene expression, a volcano plot was generated utilizing the R package "ggplot2". DEGs were determined based on the cutoffs of an adjusted P value < 0.05 and $|\log2FC| > 1$.

Identification of differentially expressed mitochondrial-related genes (DEMRGs)

By screening the MitoCarta3.0 database,[15] 1136 genes localized in mitochondria were identified. To identify expressed mitochondrial-related genes (DEMRGs), the DEGs were intersected with the mitochondrial-related genes using an online tool (https://jvenn.toulouse.inra.fr/). By utilizing the R package "ComplexHeatmap", a heatmap was generated to visualize the resulting DEMRGs.

Functional enrichment analysis

GO annotation analysis and KEGG pathway enrichment analysis of DEMRGs were conducted by utilizing R package "clusterProfiler". In addition, mitochondrial pathways (MitoPathways) were obtained from MitoCarta3.0 and analyzed using SangerBox (http://sangerbox.com/). The R package "goplot" was employed to visualize all the obtained results.

Extraction of hub DEMRGs

To identify diagnostic gene candidates, a series of analyses were performed on the DEMRGs using different machine learning algorithms. Least absolute shrinkage and selection operator (LASSO) regression was executed using the R package "glmnt" and minimal lambda value was selected as the optimal value.[16] Support vector machine recursive feature elimination (SVM-RFE) was carried out via R "kernlab" package, and the combination that resulted in the lowest errors was defined as optimal genes.[17] Gradient boosting machine (GBM) analysis was carried out utilizing the R package "gbm" and the top 10 genes were selected as optimal ones.[18] Random forest (RF) model was created using the R package "randomForest".[19] The hub DEMRGs were determined by overlapping the diagnostic gene candidates from the 4 machine learning algorithms, and then visualized in a Venn diagram.

Establishment of a diagnostic model

To assess the performance and utility of the hub DEMRGs, the package "pROC" was utilized to generate receiver operating characteristic (ROC) curves. The predictive capability of algorithms was quantified by calculating the area under the curve (AUC). Furthermore, a nomogram was constructed to predict the risk of CRSwNP by incorporating the hub DEMRGs. The effectiveness of the nomogram was evaluated by estimating its predictive accuracy using calibration curves.

Creation of network between hub genes, miRNAs and transcription factors (TFs)

We employed the NetworkAnalyst webserver (https://www.networkanalyst.ca/) to explore the regulatory network that govern hub genes, miRNAs, and TFs. Following this, we utilized Cytoscape software to visualize the network.

Immune infiltration analysis

To visualize the distribution of immunocytes in the CRSwNP and control groups, we utilized the CIBERSORT algorithm, a deconvolution algorithm designed for the analysis of tissue-infiltrating immune cell composition using signature gene matrix.[20] Additionally, we conducted Spearman correlation analysis to explore the relationships among various immunocyte pairs or between the hub DEMRGs and immunocytes.

Evaluation of MitoPathways

We obtained the pathways associated with the mitochondria from MitoCarta3.0. To explore the relationships between the mitochondrial respiratory chain and the hub DEMRGs, we conducted Spearman correlation analysis. Furthermore, we employed the single-sample gene set enrichment analysis (ssGSEA) algorithm to evaluate the activity of 149 MitoPathways in each specimen.[21] Among the results, we selected the top 10 MitoPathways with the highest variance for further investigation.

Validation in external dataset

To examine the expression of hub DEMRGs and MitoPathways, we conducted an analysis on the dataset GSE23552. Furthermore, we determined the expression levels of these hub DEMRGs in distinct cell types by analyzing the scRNA-seq dataset SCP253 using the "Seurat" package V4.3.2. Rigorous quality control protocols were implemented to exclude cells that did not meet the predefined criteria. Specifically, cells with a gene count between 200 and 6000 and a mitochondrial gene content below 5% were retained. Subsequently, data normalization was performed using the "NormalizeData" function. The 2000 genes with the highest variability were identified using the "FindVariableFeatures" function. These genes were further analyzed using principal component analysis (PCA), cluster analysis, and Uniform Manifold Approximation and Projection (UMAP) for dimensionality reduction. Differential expression analysis was conducted using the "FindAllMarkers" function, with a threshold of $|\log2FC| > 0.25$ and an adjusted P value < 0.05. The clusters were annotated based on the previous study.[22] The average expression levels of hub DEMRGs in epithelial cell genes were calculated across samples and visualized in the boxplot and heatmap.

Clinical data collection

This study received approval from the Ethics Committee of the First Affiliated Hospital of Nanjing Medical University (2020-SR-500). A total of 25 participants were included, comprising 15 CRSwNP patients and 10 control subjects. Nasal polyp specimens were procured from CRSwNP patients, whereas normal tissues from individuals who underwent septoplasty without exhibiting any symptoms of rhinosinusitis. The diagnosis of CRSwNP was based on the guidelines outlined in the European Position Paper on Rhinosinusitis and Nasal Polyps 2020.[23] Preoperative evaluation included computed tomography (CT) and endoscopic endonasal evaluation, while the Lund-Mackay scores and Lund-Kennedy scores were recorded by 2 rhinologists independently. Details regarding the participants are shown in Supplementary Table 2.

Real-time quantitative PCR

The tissue samples were subjected to total RNA isolation using FreeZol Reagent (Vazyme, Nanjing, China). RNA was subjected to reverse transcription on the HiScript III All-in-one RT SuperMix Perfect (Vazyme, Nanjing, China) to generate cDNA. qPCR analysis was conducted on a StepOnePlus System utilizing SYBR qPCR Master Mix (Vazyme, Nanjing, China). The relative gene expression, normalized to *B2M* expression, was determined employing the $2^{-\Delta\Delta Ct}$ methodology. The specific primer sequences employed in this study are shown in Supplementary Table 3. The experiment was replicated 3 times to ensure reproducibility.

Immunohistochemistry staining

Immunohistochemical staining was performed by deparaffinizing and rehydrating tissue sections (5 μm thick) using a gradient concentration of ethanol (100-75%). Antigen retrieval was accomplished by 10 mM sodium citrate buffer solution. After obstructing nonspecific antigens with 5% BSA, the slides were subjected to incubation with the primary antibodies including OXR1 (1:200, 13514-1-AP, Proteintech, Wuhan, China), BCKDHB (1:100, 13685-1-AP, Proteintech, Wuhan, China), CBR3 (1:100, 15619-1-AP, Proteintech, Wuhan, China), ALDH1L1 (1:200, 17390-1-AP, Proteintech, Wuhan, China) and HMGCS2 (1:100, A14244, Abclonal, Wuhan, China). After detection with the horseradish peroxidase-conjugated secondary antibody (PR30011, Proteintech, Wuhan, China), the slides were developed using diaminobenzidine and counterstained with hematoxylin. All the results were photographed using a microscope and then analyzed utilizing Image J software.

Isolation of primary human nasal epithelial cells (hNECs)

During the surgical procedure, nasal tissues were obtained from polyps in individuals diagnosed with CRSwNP and from inferior turbinate of the control subjects. The tissues were enzymatically digested by overnight incubation in a mixture of DMEM/F12 fortified with penicillin (200 U/mL), streptomycin (200 mg/mL), and 0.2% dispase II (Roche, Basel, Switzerland). After digestion, the nasal tissues were sieved through a 70 μm cell strainer and then centrifuged at 200 g for 3 min. The resultant sediment was suspended in PneumaCult-Ex Medium (Stemcell, Vancouver, BC, Canada) and plated onto plastic culture dishes. The culture medium was refreshed on the first day post-seeding and subsequently every other day. Having reached approximately 80% confluence, the cells were subcultured following trypsinization, and generations F1 to F3 were used for experiments.

Western blotting

Following RIPA lysis, the protein concentration of human nasal epithelial cells (hNECs) was determined. Approximately 30 μg of protein was then separated through the utilization of sodium dodecyl sulfate-polyacrylamide gel electrophoresis (SDS-PAGE). The proteins were subsequently translocated onto membranes composed of polyvinylidene difluoride (PVDF). Following the blocking by 5% BSA, the membranes were subjected to incubation with primary antibodies, including OXR1 (1:4000, 13514-1-AP, Proteintech, Wuhan, China), BCKDHB (1:1000, 13685-1-AP, Proteintech, Wuhan, China), CBR3 (1:4000, 15619-1-AP, Proteintech, Wuhan, China), ALDH1L1 (1:4000, 17390-1-AP, Proteintech, Wuhan, China), HMGCS2 (1:1000, A14244, Abclonal, Wuhan, China), and β-Actin (1:2000, #4967, Cell Signaling Technology, Danvers, MA, USA). After incubation with secondary antibodies, the binding of target proteins was visualized via the ECL system, followed by analysis utilizing Image J software.

Detection of branched chain amino acids (BCAA)

Following the manufacturer's guidelines, the BCAA levels were assessed using the BCAA kit (MAK003, Sigma-Aldrich, St Louis, MO, USA). The nasal polyps and normal mucosal tissues were weighed and homogenized, then the BCAA concentration was detected using 200 μL of the Assay buffer.

Statistical analysis

In this investigation, we utilized R software (version 4.3.1) for statistical computations and visualization of bioinformatics datasets. Additionally, GraphPad Prism (San Diego, CA, USA) and SPSS (IBM SPSS, Chicago, IL, USA) were used to analyze our experimental data delineated as mean ± standard deviation (SD). Binary comparisons were addressed using the *t*-test, while multiple group assessments using one-way ANOVA. A threshold of $P < 0.05$ was established for statistical significance.

RESULTS

Identification of DEGs between CRSwNP and control samples

The study protocol is outlined in the flow chart (Fig. 1). After mitigating the influence of batch effects, 48 samples from CRSwNP patients and 34 control samples were combined for analysis (Fig. 2A). A total of 1322 genes were identified as DEGs, comprising 737 upregulated and 585 downregulated (Fig. 2B). A Venn diagram (Fig. 2C) and a heatmap (Fig. 2D) were utilized to visualize the 24 DEMRGs obtained from the intersection of DEGs with mitochondrial-related genes. The majority of these genes exhibited a lower expression level in CRSwNP samples, compared to control samples. To assess the functional enrichment of DEMRGs, we performed GO, KEGG, and MitoCarta3.0 pathway enrichment analyses, revealing that the DEMRGs were involved in diverse biological processes, including "Mitochondrial matrix", "Arginine and proline metabolism" and "Small molecule catabolic process" (Fig. 2E). Additionally, the KEGG analysis unveiled the enrichment of DEMRGs in various pathways associated with metabolism and biosynthesis (Fig. 2E). Furthermore, using the MitoCarta3.0 database, the pathways associated with DEMRGs were explored. The findings indicated a significant connection between the DEMRGs and such pathways as "Amino acid metabolism", "Folate and 1-C metabolism" and "Vitamin metabolism" (Fig. 2F).

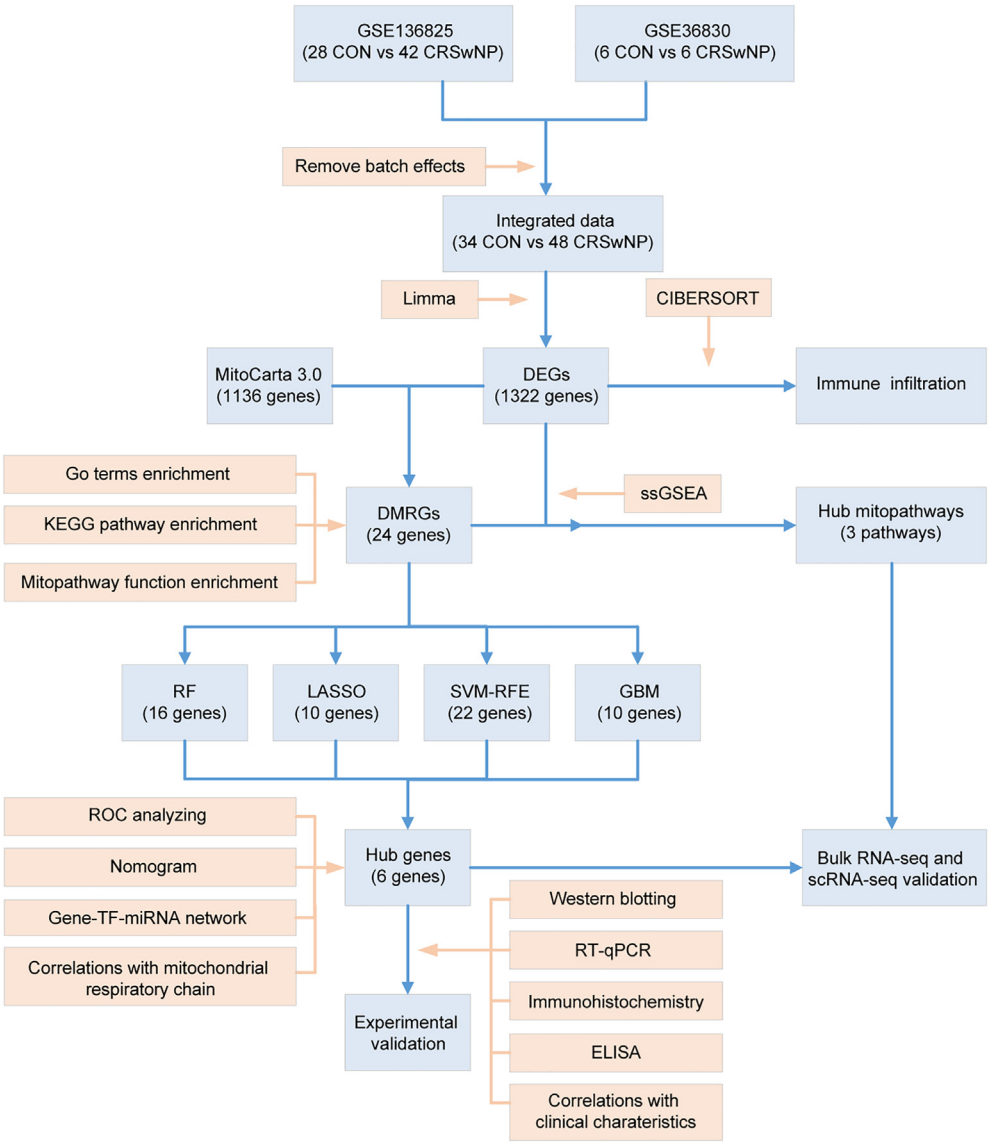

Fig. 1 The flowchart illustrating the investigative procedure. CON, control; CRSwNP, chronic rhinosinusitis with nasal polyps.

Extraction of hub DEMRGs

In order to extract the hub DEMRGs, we utilized the aforementioned set of 24 genes as inputs in 4 distinct machine learning algorithms, including LASSO regression (Fig. 3A and B), SVM-RFE algorithm (Fig. 3C), GBM algorithm (Fig. 3D), and RF algorithm (Fig. 3E). By intersecting the outputs of these algorithms, we successfully identified 6 hub DEMRGs, consisting of *ALDH1L1*, *BCKDHB*, *C15orf48*, *CBR3*, *HMGCS2*, and *OXR1* (Fig. 3F). *C15orf48* was found highly expressed in the CRSwNP samples, whereas the others in the control samples (Fig. 3G). The ROC curves for *ALDH1L1*, *BCKDHB*, *C15orf48*, *CBR3*, *HMGCS2* and *OXR1* exhibited AUCs of 0.858, 0.886, 0.807, 0.869, 0.873, and 0.912, respectively (Fig. 3H). Furthermore, the combined model achieved an AUC of 0.958, significantly higher than that of any single gene. Subsequently, a nomogram was developed to further investigate the clinical significance of these biomarkers (Fig. 3I). The calibration curves showed that the probability predicted by the nomogram was closely aligned with that of the ideal model, suggesting that these biological markers possessed a high predictive accuracy (Fig. 3J).

Network between hub genes, miRNAs and TFs

By analyzing the relationship between hub genes, miRNAs and transcription factors (TFs), we

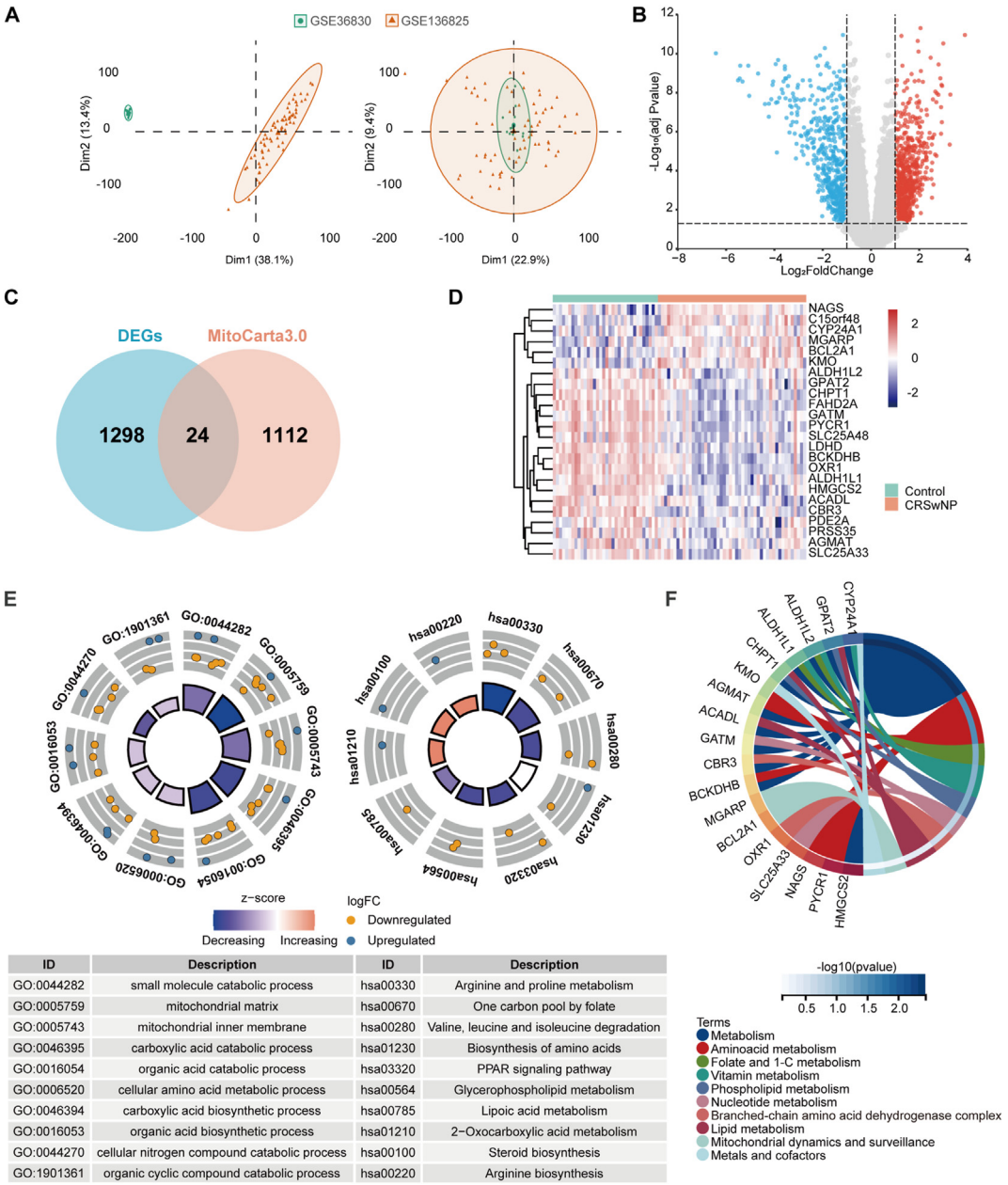

ID	Description	ID	Description
GO:0044282	small molecule catabolic process	hsa00330	Arginine and proline metabolism
GO:0005759	mitochondrial matrix	hsa00670	One carbon pool by folate
GO:0005743	mitochondrial inner membrane	hsa00280	Valine, leucine and isoleucine degradation
GO:0046395	carboxylic acid catabolic process	hsa01230	Biosynthesis of amino acids
GO:0016054	organic acid catabolic process	hsa03320	PPAR signaling pathway
GO:0006520	cellular amino acid metabolic process	hsa00564	Glycerophospholipid metabolism
GO:0046394	carboxylic acid biosynthetic process	hsa00785	Lipoic acid metabolism
GO:0016053	organic acid biosynthetic process	hsa01210	2−Oxocarboxylic acid metabolism
GO:0044270	cellular nitrogen compound catabolic process	hsa00100	Steroid biosynthesis
GO:1901361	organic cyclic compound catabolic process	hsa00220	Arginine biosynthesis

Fig. 2 Identification of the differentially expressed mitochondrial-related genes (DEMRGs) between CRSwNP and control groups. (A) PCA revealing a batch effect between the integrated datasets both before and after de-batching. (B) The volcano plot of the differentially expressed genes (DEGs). (C) The Venn diagram showing intersection genes between DEGs and Mitochondrial-related genes from MitoCarta3.0. (D) Clustered heatmap of DEMRGs. (E) GO and KEGG pathway enrichment analyses of DEMRGs. (F) MitoPathway enrichment analysis of DEMRGs.

conducted a network to identify the essential miRNAs and TFs implicated in the mechanism of CRSwNP (Fig. 4). This network consisted of 93 miRNAs, 6 mRNAs, 43 TFs, 142 nodes, and 181 edges. *OXR1* was found to be the top targeted gene, modulated by 71 miRNAs and 13 TFs. Hsa-mir-182-5p was the miRNA regulating the highest number of DEMRGs. Furthermore, *PPARG* and *STAT3* were identified as the TFs regulating the largest number of DEMRGs.

Immune cell infiltration analysis

Five groups of immunocytes demonstrated notable variations between the nasal polyps and normal nasal tissues (Fig. 5A). Specifically, resting mast cells, M2 macrophages and resting dendritic cells (DCs) were significantly enriched in CRSwNP samples. On the other hand, plasma cells and M0 macrophages were much more abundant in control samples (Fig. 5B). Further

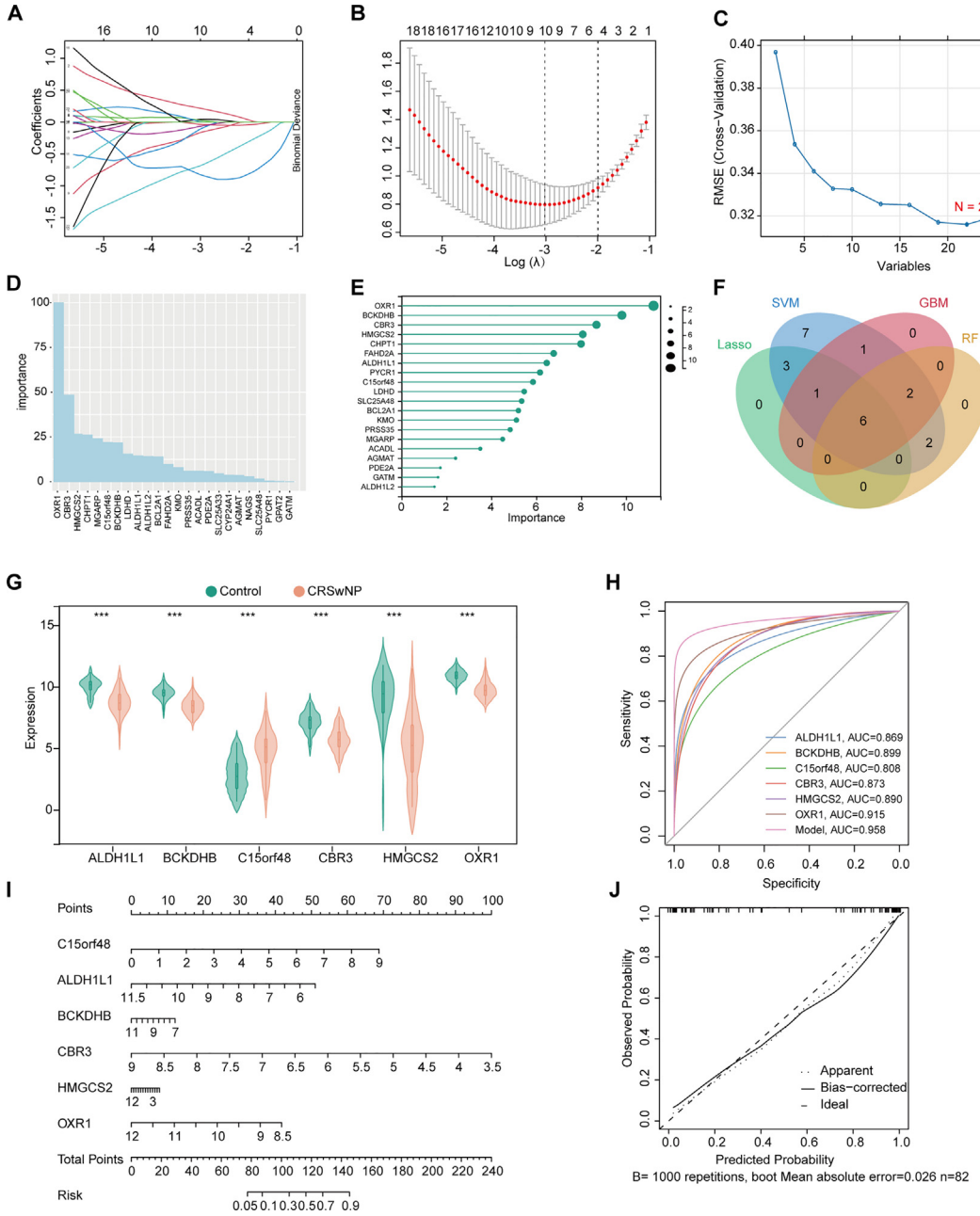

Fig. 3 Detection of hub DEMRGs utilizing a comprehensive methodology. (A, B) Implementation of the LASSO regression. (C) Tenfold cross-validation error estimated using SVM-RFE. (D) The importance of features according to GBM algorithm. (E) Biomarker screening using the RF algorithm. (F) Venn diagram illustrating the intersection among the 4 above-mentioned machine learning outputs. (G) The expression of hub DEMRGs in CRSwNP and control samples. (H) The ROC curve of the diagnostic efficacy of the hub DEMRGs. (I) A nomogram model based on the 6 diagnostic biomarkers. (J) The calibration curve of the nomogram assessing the prognostic accuracy of the model. **P* < 0.05; ***P* < 0.01; ****P* < 0.001; *****P* < 0.0001; ns, not significant.

analysis of immune cell infiltration revealed several significant associations among various cellular subtypes (Fig. 5C). Spearman correlation analysis revealed a consistently positive correlation of the expression levels of *ALDH1L1*, *BCKDHB*, *CBR3*, *HMGCS2* and *OXR1* with the abundance of M2 macrophages and resting mast cells. Conversely, their expression levels showed a coherently negative correlation with the infiltration of plasma cells and M0 macrophages. *C15orf48* displayed a markedly positive correlation with memory activated CD4 T cells and M2 macrophages, but a negative correlation with M0 macrophages (Fig. 5D).

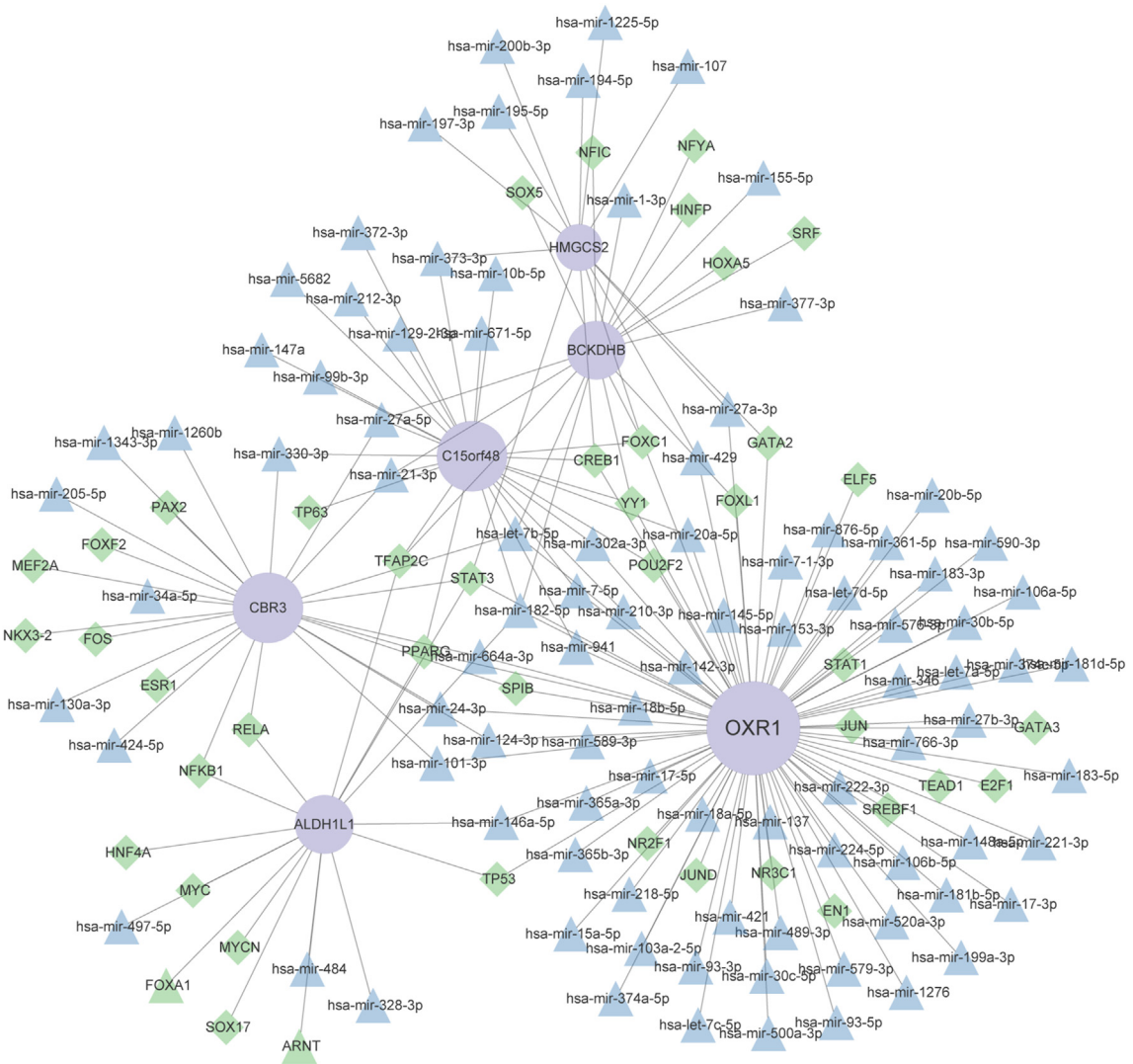

Fig. 4 Target gene-miRNA and target gene-transcription factor (TF) networks are depicted in the diagram. Genes are represented by purple circled nodes, miRNAs by blue triangle nodes, and TFs by green diamond nodes.

Mitochondrial characteristics in CRSwNP

The top 10 MitoPathways were selected based on their log2FC values using the ssGSEA algorithm, all of which displayed a decreased activity in CRSwNP (Fig. 6A). By integrating the top 10 MitoPathways with the MitoPathways via MitoCarta3.0 pathway enrichment analysis, 3 hub MitoPathways including "Amino acid metabolism", "Phospholipid metabolism" and "Branched-chain amino acid dehydrogenase complex" were identified (Fig. 6B). An assessment was carried out to investigate the correlation between DEMRGs and genes linked to the respiratory chain complexes (I–V) (Fig. 6C). A robust positive correlation was observed between the expression levels of respiratory chain complex genes and *HMGCS2*.

Expression of hub DEMRGs in validation datasets

The analysis of dataset GSE23552 revealed that the expression levels of *ALDH1L1*, *BCKDHB*, *CBR3*, *HMGCS2*, and *OXR1* were significantly lower in nasal polyps compared to normal nasal mucosa (Fig. 7A). In contrast, the expression levels of *C15orf48* remained unchanged between the 2 cohorts. Furthermore, activities of major MitoPathways, specifically "Amino acid metabolism" and "Branched-chain amino acid dehydrogenase complex", were significantly repressed in CRSwNP samples (Fig. 7B). Subsequent scRNAseq analysis highlighted that

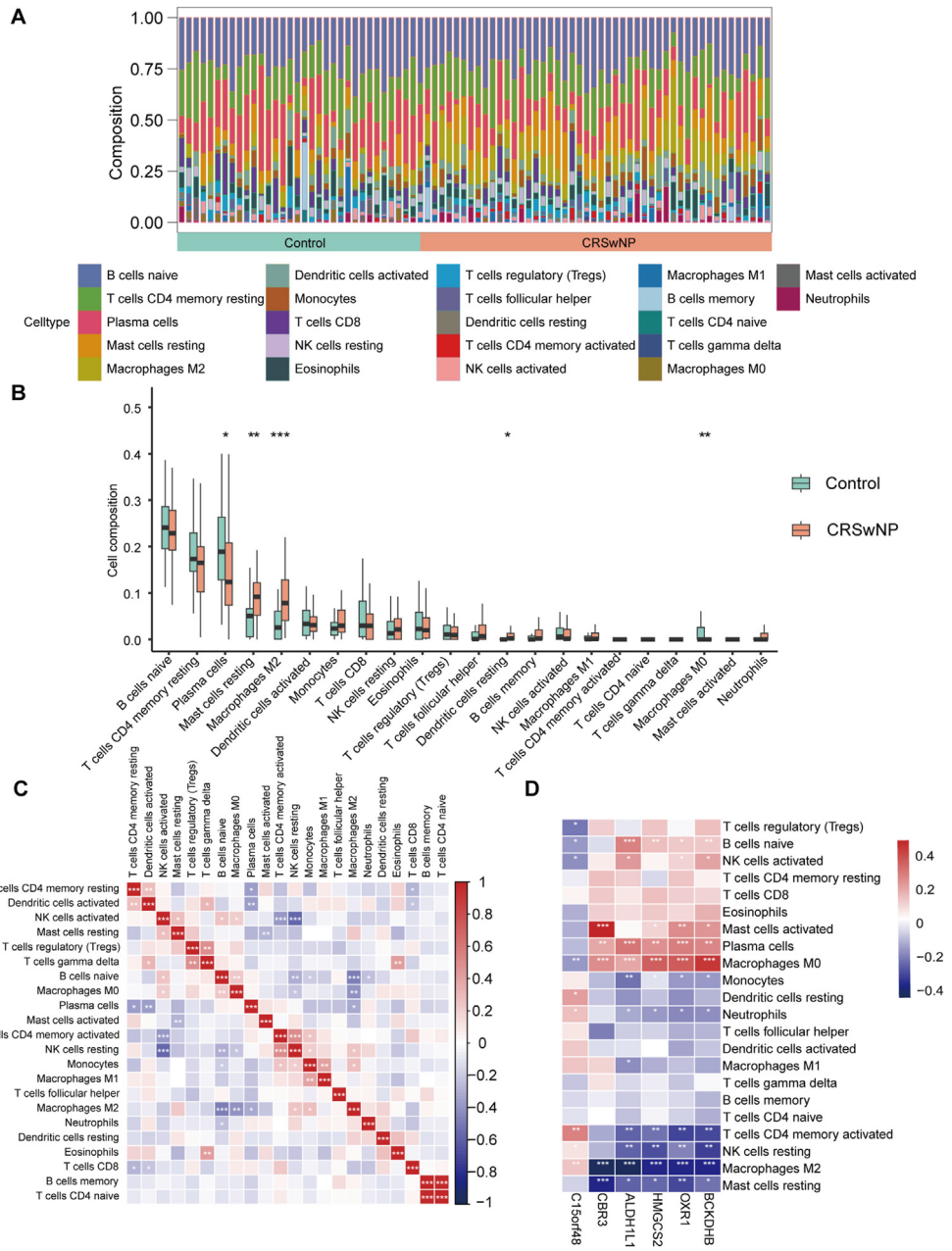

Fig. 5 Comparison of immune cell infiltration between CRSwNP and control groups. (A) The stacked bar chart illustrating the distribution of immune cell types. (B) The box plot depicting the contrasting distribution of 22 distinct types of immune cells between the CRSwNP and control groups. (C) The heatmap displaying the correlation patterns among the 22 types of infiltrating immune cells. (D) The correlation map showing the connection between differentially infiltrating immune cells and hub DEMRGs. *****$P < 0.05$; ******$P < 0.01$; *******$P < 0.001$; ********$P < 0.0001$; ns, not significant.

C15orf48 was predominantly expressed in myeloid cells, but the other hub genes in epithelial cells (Fig. 7C–D). The downregulation of these genes in nasal polyp epithelial cells was consistent with findings from previous analysis (Fig. 7E–F).

Negative correlation between the expression of hub DEMRGs and CRSwNP severity

The results of RT-qPCR indicated that the expression levels of *ALDH1L1*, *BCKDHB*, *CBR3*, *HMGCS2*, and *OXR1* were significantly decreased

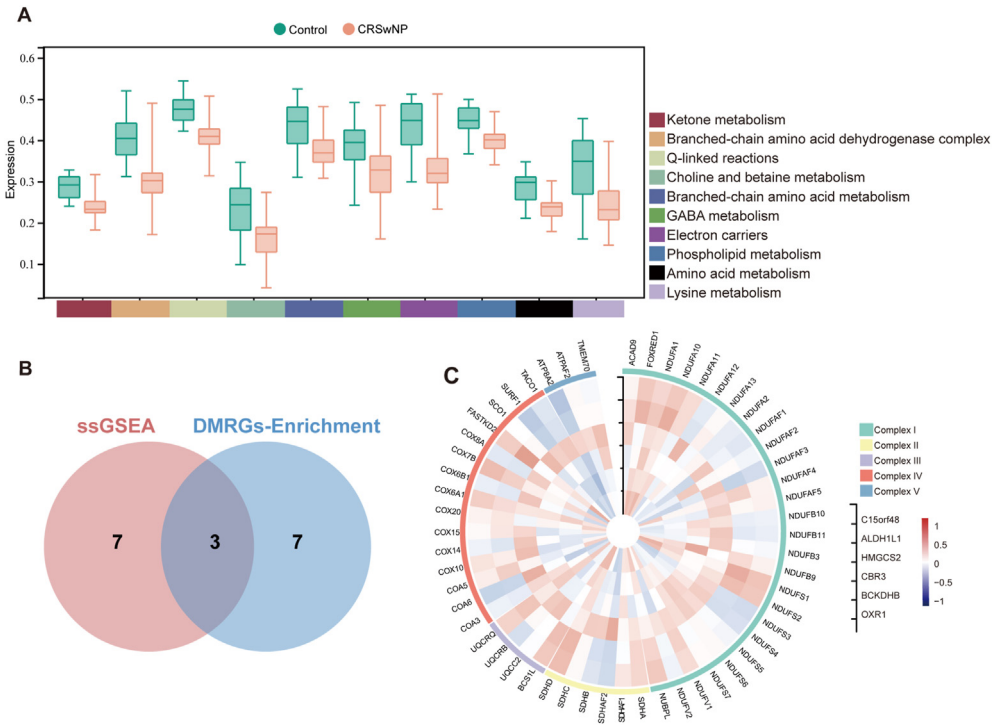

Fig. 6 MitoPathway-related characteristics in CRSwNP. (A) Distinct ssGSEA scores of the top 10 MitoPathways between CRSwNP and control samples. (B) Hub MitoPathways by intersecting the top 10 MitoPathways with the DEMRGs enrichment results. (C) Correlation between hub DEMRGs and respiratory chain complex (I–V) genes.

in CRSwNP samples (Fig. 8A). To investigate the relationship between the hub DEMRGs and the severity of CRSwNP, the Lund-Mackay and Lund-Kennedy scores of patients with CRSwNP were evaluated (Supplementary Table 4). The Lund-Mackay score had significantly positive correlations with the ΔCt values of *ALDH1L1* ($R^2 = 0.45$; $P = 0.005$), *BCKDHB* ($R^2 = 0.48$; $P = 0.042$), *CBR3* ($R^2 = 0.47$; $P = 0.011$), *HMGCS2* ($R^2 = 0.30$; $P = 0.032$), *OXR1* ($R^2 = 0.41$; $P = 0.006$) (Fig. 8B). Similarly, The Lund-Kennedy score displayed significantly positive correlations with the ΔCt of *ALDH1L1* ($R^2 = 0.47$; $P = 0.006$), *BCKDHB* ($R^2 = 0.28$; $P = 0.004$), *CBR3* ($R^2 = 0.40$; $P = 0.005$), *HMGCS2* ($R^2 = 0.31$; $P = 0.033$), *OXR1* ($R^2 = 0.45$; $P = 0.010$) (Fig. 8B).

Nasal polyps exhibit reduced protein expression levels of DEMRGs

Immunohistochemistry and Western blotting showed a significant decrease in the protein levels of ALDH1L1, BCKDHB, CBR3, HMGCS2, and OXR1 in both nasal polyp tissues and hNECs derived from these polyps (Fig. 8C–F). Additionally, the concentrations of BCAA elevated significantly in nasal polyps, compared to the normal nasal mucosa (Fig. 8G).

DISCUSSION

CRSwNP, a multifactorial condition, has an etiology involving genetic, anatomical, and environmental components. Prior investigations have demonstrated that dysregulation of mitochondrial function in nasal epithelial cells may induce the pathogenesis of CRSwNP.[5] However, the molecular mechanisms underlying this phenomenon remain undefined. In this investigation, we utilized public datasets from the GEO database to identify the DEMRGs between CRSwNP patients and control subjects. By applying integrated machine learning methods, we pinpointed 5 genes: *ALDH1L1*, *BCKDHB*, *CBR3*, *HMGCS2*, and *OXR1*. The downregulation of these genes was subsequently validated through external datasets and laboratory experiments. Furthermore, we observed a significant association between the downregulation of these genes and the heightened severity of CRSwNP.

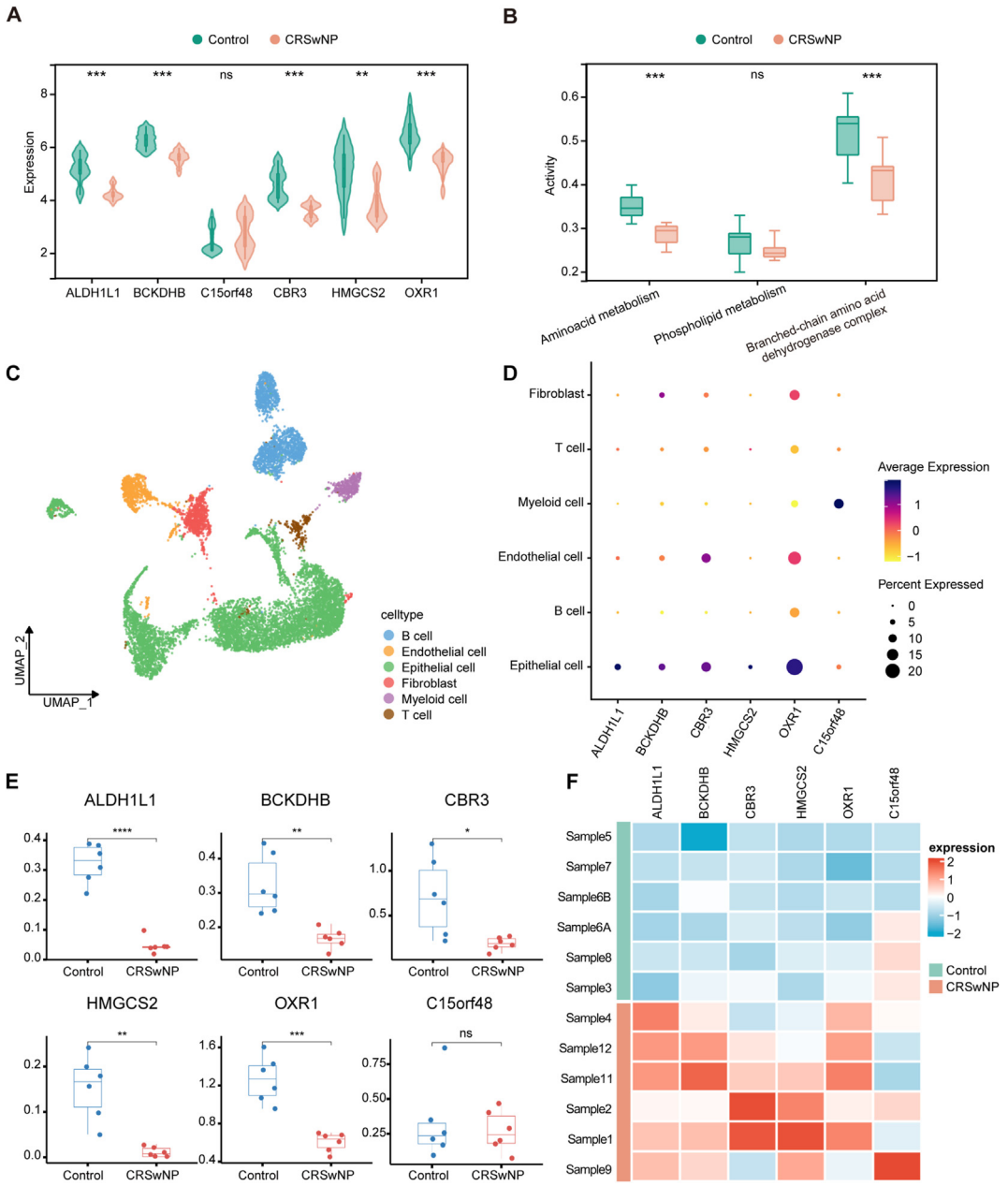

Fig. 7 The expression of biomarkers between CRSwNP and control groups in validation datasets. (A) The expression of hub DEMRGs in GSE23552. (B) The expression of hub MitoPathways in GSE23552. (C) The UMAP map showing annotation results of cell subgroups in the scRNAseq data. (D) The distribution of hub DEMRGs in 6 cell subgroups. (E, F) The mean expression of hub DEMRGs in epithelial cells for each individual sample. *****$P < 0.05$; ******$P < 0.01$; *******$P < 0.001$; ********$P < 0.0001$; ns, not significant.

Cytosolic 10-formyltetrahydrofolate dehydrogenase (ALDH1L1) serves as an essential enzyme in the folate metabolic pathway. By breaking down harmful intracellular aldehyde compounds, ALDH1L1 effectively reduces oxidative stress, a major contributor to the development of CRSwNP. Additionally, ALDH1L1 regulates the expression of cell cycle-related gene via its metabolic capabilities. Recent investigations have revealed that the re-expression of ALDH1L1 not only hampers cellular proliferation, but also the migration and invasion of cancer cells.[23,24] Given the critical role of tissue restructuring in the pathogenesis of CRSwNP, ALDH1L1 emerges as a promising indicator for the progression of nasal polyp growth.

Branched chain keto acid dehydrogenase E1 subunit beta (BCKDHB) performs an important role in metabolizing BCAA within the human body. The

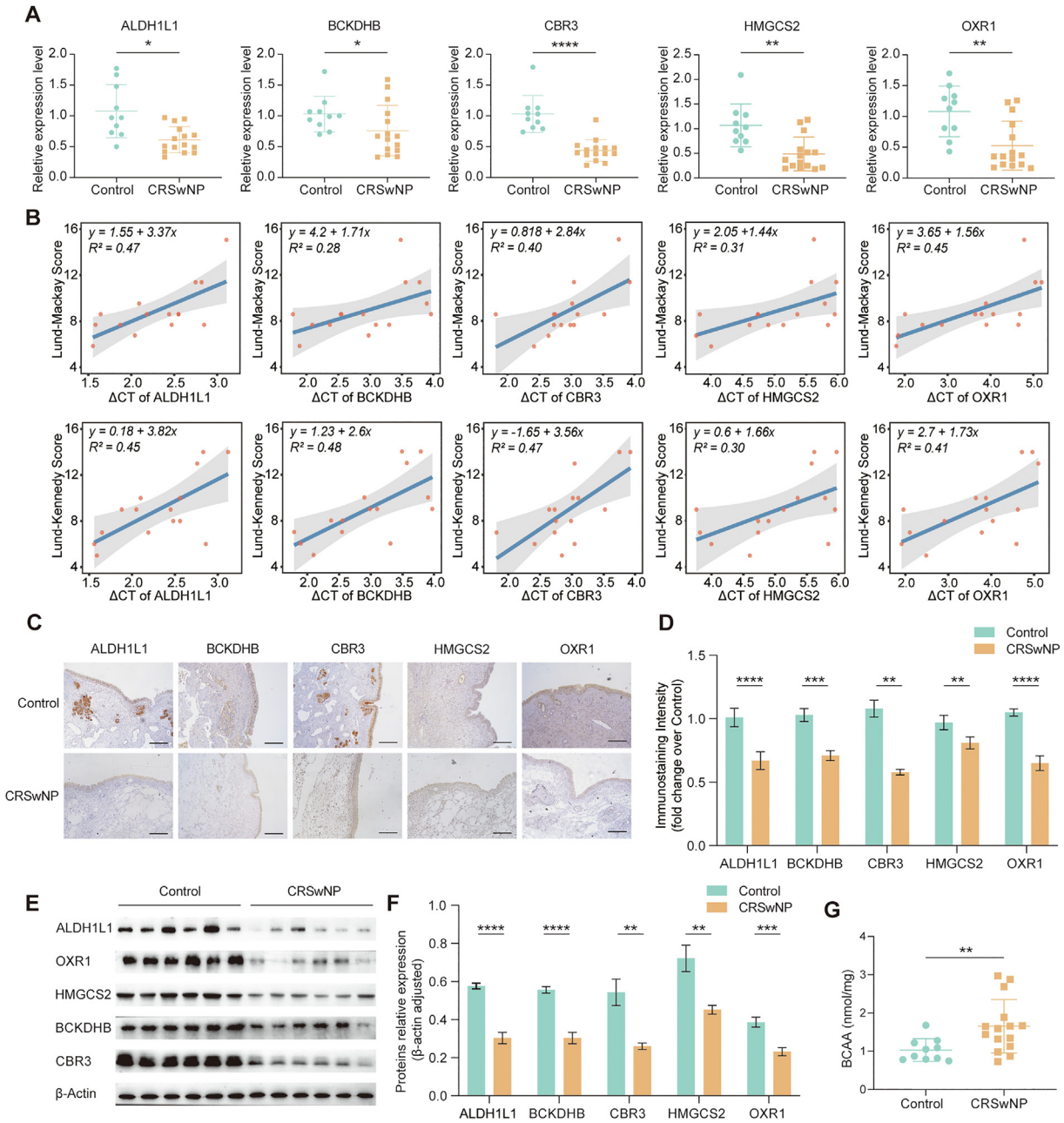

Fig. 8 Confirmation of *ALDH1L1*, *BCKDHB*, *CBR3*, *HMGCS2*, and *OXR1* expression and their association with the severity of CRSwNP. (A) mRNA expression of hub DEMRGs in CRSwNP and control samples. (B) Correlations between the ΔCt in PCR of hub DEMRGs and the severity of CRSwNP, including Lund-Mackey score and Lund-Kennedy score. (C, D) Immunostaining of protein expression. Scale bars = 200 μm. (E, F) Representative expression levels of hub DEMRGs in Western blotting. (G) BCAA concentrations in nasal mucosa from CRSwNP and control groups. ΔCt = Ct (DEMRGs) – Ct (*B2M*); *$P < 0.05$; **$P < 0.01$; ***$P < 0.001$; ****$P < 0.0001$; ns, not significant.

role of BCKDHB in BCAA metabolism is associated with inflammatory responses and immune function. Impairment in BCKDHB function can elevate oxidative stress, leading to excessive generation of free radical. Such oxidative imbalance can cause cellular damage and tissue inflammation, thereby promoting the advancement of CRSwNP. Previous studies have indicated that individuals with severe asthma exhibit higher plasma BCAA levels, compared to those with mild asthma.[25] Considering the close association between CRSwNP and asthma, BCKDHB might contribute

to the development of CRSwNP by promoting abnormal accumulation of BCAA and their metabolites.

Carbonyl reductase 3 (CBR3) is an NADPH-dependent enzyme that primarily catalyzes the reduction of various endogenous and exogenous carbonyl compounds. Bioinformatic analysis has revealed an association between CBR3 and both chronic obstructive pulmonary disease (COPD) and exposure to cigarette smoke, indicating that CBR3 could serve as a potential diagnostic biomarker for airway inflammatory diseases.[26] Furthermore, genetic variations in CBR3 have been associated with the progression of several inflammatory conditions, including rheumatoid arthritis, chronic nephritis, and inflammatory bowel disease.[27] Consequently, dysfunction in CBR3 may impair the body's antioxidant defenses, thereby heightening the risk of developing CRSwNP.

3-Hydroxy-3-methylglutaryl-CoA synthase 2 (HMGCS2) plays a crucial role in mitochondrial function, significantly impacting both energy and lipid metabolism. In the ketogenesis pathway, HMGCS2 catalyzes the production of β-hydroxybutyrate, a ketone body known to inhibit the NLRP3 inflammasome.[28] This inhibition reduces the secretion of pro-inflammatory cytokines like IL-1β and IL-18, thereby alleviating oxidative stress and inflammation within nasal epithelial cells. Additionally, HMGCS2 is involved in the differentiation of epithelial cells and the regulation of tight junction proteins, which are vital for maintaining the integrity of the epithelial barrier.[29]

Oxidation resistance 1 (OXR1) is fundamental to the stabilization of intracellular redox states, providing a robust defense against oxidative stress. Genetic studies have revealed that polymorphisms in the OXR1 gene are associated with the development of allergic asthma in children, suggesting a potential link to airway inflammatory diseases.[30] Recent research indicates that the expression levels of OXR1 are reduced in epithelial cells of nasal polyps compared to healthy nasal mucosa which increase susceptibility to oxidative stress and exacerbate inflammatory responses.[31]

Immune dysregulation plays a pivotal role in the pathogenesis of CRSwNP. Our current research utilized the CIBERSORT algorithm to assess immune cell infiltration in nasal tissues, revealing increased abundances of M2 macrophages, resting DCs, and mast cells. Notably, M2 macrophages emerge as a pivotal player in the tissue remodeling in CRSwNP, particularly through the release of growth factors that promote fibroblast proliferation and the degradation of the extracellular matrix.[32,33] Additionally, M2 macrophages are instrumental in modulating anti-inflammatory responses and promoting type 2 immune responses.[34] Recent findings highlight a significant increase in mast cells within nasal polyps, predominantly localized to the epithelium, where they facilitate tissue remodeling by releasing carboxypeptidase A3.[35] Furthermore, the presence of mast cells may enhance the recruitment of eosinophils, thereby amplifying type 2 inflammatory responses.[36] Flow cytometry studies by Zhai et al[37] have substantiated a positive correlation between the presence of eosinophils and mast cells in patients with CRSwNP, corroborating the outcomes of our analysis on immune infiltration. In the microenvironment of nasal polyps, a marked increase in DC infiltration significantly elevates Th2 cytokines levels, thereby disturbing the Th1/Th2 balance.[38,39] Aligning with our results, a recent scRNA-seq analysis by Wang et al[40] has demonstrated high expression levels of DC markers *CD163* and *NR4A1* in early CRSwNP, potentially contributing to T cell activation. Furthermore, research by Lin et al[41] has identified that DCs expressing *CD80* and *CD86* exacerbate CRSwNP inflammation through interactions with *CD40L* on T cells, promoting T cell maturation and the release of inflammatory molecules. Previous research has highlighted the critical role of mitochondrial metabolism in shaping the function and destiny of immune cells.[42] Our correlational studies revealed that the hub DEMRGs are inversely related to M2 macrophages and mast cells, suggesting that mitochondrial dysregulation may amplify type 2 inflammation by facilitating the infiltration of these cells in the nasal epithelium. Additionally, we observed a positive correlation between the expression levels of all 5 hub genes with M0 macrophages and plasma cells. M0 macrophages, initially in a quiescent state, have potential to differentiate into either M1 or M2

macrophages in response to environmental stimuli. Our study demonstrated that in nasal polyps, the loss of function of the mitochondrial-related genes facilitated the transition from M0 to M2 macrophages. Plasma cells, which are the terminal differentiation stage of B cells, exhibit high metabolic activity and require substantial energy to maintain their immune functions.[43] Reduced expression of mitochondrial-related genes may impair the survival and function of plasma cells by limiting energy supply and weakening antioxidant defenses, ultimately affecting their abundances in nasal polyps.

In this study, we employed 2 algorithms to identify differentially activated metabolic pathways between nasal polyps and normal mucosa. Our findings demonstrated a downregulation of BCAA in the CRSwNP group. Previous research indicates that BCAA is implicated in modulating the metabolism of glucose, lipids, and proteins.[44] Furthermore, BCAA can facilitate interorgan metabolic communication, suggesting that abnormalities in BCAA catabolism may contribute to the progression of diverse metabolic disorders.[45] However, the correlation between BCAA metabolism and airway inflammatory diseases has been underexplored. Comhair et al[25] have reported that the level of plasma BCAA increases in asthmatics with elevated levels of fractional exhaled nitric oxide (FENO), compared to those with low FENO levels. Conversely, Li et al[46] have revealed the upregulation of branched-chain amino acid transaminase 1 (BCAT1) in neonatal asthmatic mice, suggesting that inhibiting BCAT1 may attenuate airway inflammation and remodeling by reducing autophagy. The present study indicated that the metabolic disruption of BCAA might serve as a trigger for CRSwNP, thereby providing novel insights into the mechanism of upper airway inflammatory diseases.

To the best of our knowledge, this study is the first to comprehensive explore the relationship between mitochondrial dysfunction and the immune microenvironment in CRSwNP. We identified that 5 genes, namely *ALDH1L1*, *BCKDHB*, *CBR3*, *HMGCS2*, and *OXR1*, as potential molecular markers for the diagnosis and treatment of CRSwNP. However, our study has several limitations. First, the analysis was constrained by a relatively small dataset. Moreover, though we validated the expression of hub DEMRGs in human tissues, the intricate regulatory mechanisms governing these genes in CRSwNP require further elucidation through *in vivo* and *in vitro* studies.

CONCLUSION

This comprehensive bioinformatics study identifies substantial variations in mitochondrial gene expression between patients diagnosed with CRSwNP and control subjects. Specifically, *ALDH1L1, BCKDHB, CBR3, HMGCS2,* and *OXR1* regulate immune infiltration in CRSwNP. These genes might serve as prognostic and therapeutic strategies for CRSwNP.

Abbreviations

CRSwNP, chronic rhinosinusitis with nasal polyps; CRSsNP, chronic rhinosinusitis without nasal polyps; OXPHOS, oxidative phosphorylation; ATP, adenosine triphosphate; ROS, reactive oxygen species; ADMA, asymmetric dimethylarginine; GEO, Gene Expression Ominibus; DEGs, differentially expressed genes; DEMRGs, differentially expressed mitochondrial-related genes; GO, gene ontology; KEGG, Kyoto encyclopedia of genes and genomes; MitoPathways, mitochondrial pathways; LASSO, absolute shrinkage and selection operator; SVM-RFE, support vector machine recursive feature elimination; GBM, gradient boosting machine; RF, random forest; ROC, receiver operating characteristic; AUC, area under the curve; TFs, transcription factors; CIBERSORT, cell-type identification by estimating relative subsets of RNA transcripts; ssGSEA, single-sample gene set enrichment analysis; CT, computed tomography; hNECs, human nasal epithelial cells; SDS-PAGE, sodium dodecyl sulfate-polyacrylamide gel electrophoresis; PVDF, polyvinylidene difluoride; BCAA, branched chain amino acids; DCs, dendritic cells; N-ERD, nonsteroidal anti-inflammatory drug-exacerbated respiratory disease; COPD, chronic obstructive pulmonary disease; FENO, fractional exhaled nitric oxide; SEB, staphylococcal enterotoxin B.

Funding

This work was supported by the National Natural Science Foundation (82171117) and Jiangsu Province Capability Improvement Project through Science, Technology and Education (JSDW202203) of China.

Availability of data and materials

The datasets utilized in this study are accessible in online repositories. GSE136825, GSE36830, and GSE23552 can be accessed at https://www.ncbi.nlm.nih.gov/geo/. SCP253 can be accessed at https://singlecell.broadinstitute.org/single_cell/.

Author contributions

M.-P.L. and L.C. designed the study. M.G., C.H., J.-Q.Z., Y.Y., and X.-Y.Z. carried out subject enrollment and data collection. B.Y. conducted experimental work, analyzed the data, and prepared the manuscript. C.-Y.Q., M.-P.L., and L.C. interpreted the results, reviewed, and edited the manuscript. All authors provided their consent for the submission of the final version.

Ethics statement

This study obtained ethical approval from the Ethical Committee of the First Affiliated Hospital of Nanjing Medical University (2020-SR-500) for research involving human participants.

Consent for publication

The authors obtained informed consent for publication from all participants in the study. The participants understand that their personal information will not be published.

Declaration of competing interest

The authors declare that they conducted the research without any potential conflict of interest arising from commercial or financial relationships.

Acknowledgments

We express our gratitude to Professor Yun Chen (Department of Immunology, School of Basic Medical Sciences, Nanjing Medical University) for providing the necessary infrastructure to conduct our experiment. We also thank Associate Professor Yong-Ke Cao (School of Foreign Languages, Nanjing Medical University) for professional English-language proofreading of the manuscript.

Appendix A. Supplementary data

Supplementary data to this article can be found online at https://doi.org/10.1016/j.waojou.2024.100964.

Author details

[a]Department of Otorhinolaryngology & Clinical Allergy Center, The First Affiliated Hospital, Nanjing Medical University, Nanjing, China. [b]International Centre for Allergy Research, Nanjing Medical University, Nanjing, China.

REFERENCES

1. Kato A, Schleimer RP, Bleier BS. Mechanisms and pathogenesis of chronic rhinosinusitis. *J Allergy Clin Immunol*. 2022;149(5):1491–1503.
2. Fokkens WJ, Lund V, Bachert C, et al. EUFOREA consensus on biologics for CRSwNP with or without asthma. *Allergy*. 2019;74(12):2312–2319.
3. Prakash YS, Pabelick CM, Sieck GC. Mitochondrial dysfunction in airway disease. *Chest*. 2017;152(3):618–626.
4. Chellappan DK, Paudel KR, Tan NW, et al. Targeting the mitochondria in chronic respiratory diseases. *Mitochondrion*. 2022;67:15–37.
5. Yoon YH, Yeon SH, Choi MR, et al. Altered mitochondrial functions and morphologies in epithelial cells are associated with pathogenesis of chronic rhinosinusitis with nasal polyps. *Allergy Asthma Immunol Res*. 2020;12(4):653–668.
6. Wang C, Zhou ML, Liu YC, et al. The roles of autophagy, mitophagy, and the akt/mTOR pathway in the pathogenesis of chronic rhinosinusitis with nasal polyps. *J Immunol Res*. 2022;2022, 2273121.
7. Kim YM, Jin J, Choi JA, et al. Staphylococcus aureus enterotoxin B-induced endoplasmic reticulum stress response is associated with chronic rhinosinusitis with nasal polyposis. *Clin Biochem*. 2014;47(1-2):96–103.
8. Stevens WW, Peters AT, Tan BK, et al. Associations between inflammatory endotypes and clinical presentations in chronic rhinosinusitis. *J Allergy Clin Immunol Pract*. 2019;7(8):2812–2820 e3.
9. Weinberg SE, Sena LA, Chandel NS. Mitochondria in the regulation of innate and adaptive immunity. *Immunity*. 2015;42(3):406–417.
10. Aguilera-Aguirre L, Bacsi A, Saavedra-Molina A, et al. Mitochondrial dysfunction increases allergic airway inflammation. *J Immunol*. 2009 15;183(8):5379–5387.
11. Pattnaik B, Bodas M, Bhatraju NK, et al. IL-4 promotes asymmetric dimethylarginine accumulation, oxo-nitrative stress, and hypoxic response-induced mitochondrial loss in airway epithelial cells. *J Allergy Clin Immunol*. 2016;138(1):130–141 e9.
12. Peng Y, Zi XX, Tian TF, et al. Whole-transcriptome sequencing reveals heightened inflammation and defective host defence responses in chronic rhinosinusitis with nasal polyps. *Eur Respir J*. 2019;54(5), 1900732.
13. Stevens WW, Ocampo CJ, Berdnikovs S, et al. Cytokines in chronic rhinosinusitis. Role in eosinophilia and aspirin-exacerbated respiratory disease. *Am J Respir Crit Care Med*. 2015;192(6):682–694.
14. Plager DA, Kahl JC, Asmann YW, et al. Gene transcription changes in asthmatic chronic rhinosinusitis with nasal polyps and comparison to those in atopic dermatitis. *PLoS One*. 2010;5(7), e11450.
15. Rath S, Sharma R, Gupta R, et al. MitoCarta3.0: an updated mitochondrial proteome now with sub-organelle localization and pathway annotations. *Nucleic Acids Res*. 2021;49(D1):D1541–D1547.
16. Cheung-Lee WL, Link AJ. Genome mining for lasso peptides: past, present, and future. *J Ind Microbiol Biotechnol*. 2019;46(9-10):1371–1379.
17. Sanz H, Valim C, Vegas E, et al. SVM-RFE: selection and visualization of the most relevant features through non-linear kernels. *BMC Bioinf*. 2018;19(1):432.
18. Salditt M, Humberg S, Nestler S. Gradient tree boosting for hierarchical data. *Multivariate Behav Res*. 2023;58(5):911–937.

19. Wang H, Yang F, Luo Z. An experimental study of the intrinsic stability of random forest variable importance measures. *BMC Bioinf*. 2016;17:60.
20. Newman AM, Liu CL, Green MR, et al. Robust enumeration of cell subsets from tissue expression profiles. *Nat Methods*. 2015;12(5):453–457.
21. Barbie DA, Tamayo P, Boehm JS, et al. Systematic RNA interference reveals that oncogenic KRAS-driven cancers require TBK1. *Nature*. 2009;462(7269):108–112.
22. Ordovas-Montanes J, Dwyer DF, Nyquist SK, et al. Allergic inflammatory memory in human respiratory epithelial progenitor cells. *Nature*. 2018;560(7720):649–654.
23. Rodriguez FJ, Giannini C, Asmann YW, et al. Gene expression profiling of NF-1-associated and sporadic pilocytic astrocytoma identifies aldehyde dehydrogenase 1 family member L1 (ALDH1L1) as an underexpressed candidate biomarker in aggressive subtypes. *J Neuropathol Exp Neurol*. 2008;67(12):1194–1204.
24. Krupenko SA, Krupenko NI. Loss of ALDH1L1 folate enzyme confers a selective metabolic advantage for tumor progression. *Chem Biol Interact*. 2019;302:149–155.
25. Comhair SA, McDunn J, Bennett C, et al. Metabolomic endotype of asthma. *J Immunol*. 2015;195(2):643–650.
26. Lin L, Lin G, Chen X, et al. Identification of small airway epithelium-related hub genes in chronic obstructive pulmonary disease. *Int J Chronic Obstr Pulm Dis*. 2022;17:3001–3015.
27. Oppermann U. Carbonyl reductases: the complex relationships of mammalian carbonyl- and quinone-reducing enzymes and their role in physiology. *Annu Rev Pharmacol Toxicol*. 2007;47:293–322.
28. Youm YH, Nguyen KY, Grant RW, et al. The ketone metabolite β-hydroxybutyrate blocks NLRP3 inflammasome-mediated inflammatory disease. *Nat Med*. 2015;21(3):263–269.
29. Tai J, Shin JM, Park J, et al. Oxidative stress and antioxidants in chronic rhinosinusitis with nasal polyps. *Antioxidants*. 2023;12(1):195.
30. Baurley JW, Conti DV. A scalable, knowledge-based analysis framework for genetic association studies. *BMC Bioinf*. 2013;14:312.
31. Jardeleza C, Jones D, Baker L, et al. Gene expression differences in nitric oxide and reactive oxygen species regulation point to an altered innate immune response in chronic rhinosinusitis. *Int Forum Allergy Rhinol*. 2013;3(3):193–198.
32. Banks CA, Schlosser RJ, Wang EW, et al. Macrophage infiltrate is elevated in CRSwNP sinonasal tissue regardless of atopic status. *Otolaryngol Head Neck Surg*. 2014;151(2):215–220.
33. Mantovani A, Biswas SK, Galdiero MR, et al. Macrophage plasticity and polarization in tissue repair and remodelling. *J Pathol*. 2013;229(2):176–185.
34. Wang ZC, Yao Y, Wang N, et al. Deficiency in interleukin-10 production by M2 macrophages in eosinophilic chronic rhinosinusitis with nasal polyps. *Int Forum Allergy Rhinol*. 2018;8(11):1323–1333.
35. Dwyer DF, Ordovas-Montanes J, Allon SJ, et al. Human airway mast cells proliferate and acquire distinct inflammation-driven phenotypes during type 2 inflammation. *Sci Immunol*. 2021;6(56), eabb7221.
36. Zhai GT, Li JX, Zhang XH, et al. Increased accumulation of CD30 ligand-positive mast cells associates with eosinophilic inflammation in nasal polyps. *Laryngoscope*. 2019;129(3):E110–E117.
37. Zhai GT, Wang H, Li JX, et al. IgD-activated mast cells induce IgE synthesis in B cells in nasal polyps. *J Allergy Clin Immunol*. 2018;142(5):1489–1499 e23.
38. Ito T, Liu YJ, Arima K. Cellular and molecular mechanisms of TSLP function in human allergic disorders–TSLP programs the "Th2 code" in dendritic cells. *Allergol Int*. 2012;61(1):35–43.
39. Cao PP, Shi LL, Xu K, et al. Dendritic cells in inflammatory sinonasal diseases. *Clin Exp Allergy*. 2016;46(7):894–906.
40. Wang Y, Song X, Jin M, Lu J. Characterization of the immune microenvironment and identification of biomarkers in chronic rhinosinusitis with nasal polyps using single-cell RNA sequencing and transcriptome analysis. *J Inflamm Res*. 2024;17:253–277.
41. Lin X, Zhuang X, Li C, et al. Interactions between dendritic cells and T lymphocytes in pathogenesis of nasal polyps. *Exp Ther Med*. 2018;15(6):5167–5172.
42. Makowski L, Chaib M, Rathmell JC. Immunometabolism: from basic mechanisms to translation. *Immunol Rev*. 2020;295(1):5–14.
43. Cyster JG, Allen CDC. B cell responses: cell interaction dynamics and decisions. *Cell*. 2019;177(3):524–540.
44. Nie C, He T, Zhang W, et al. Branched chain amino acids: beyond nutrition metabolism. *Int J Mol Sci*. 2018;19(4):954.
45. Gancheva S, Jelenik T, Álvarez-Hernández E, et al. Interorgan metabolic crosstalk in human insulin resistance. *Physiol Rev*. 2018;98(3):1371–1415.
46. Li J, Chen M, Lu L, et al. Branched-chain amino acid transaminase 1 inhibition attenuates childhood asthma in mice by effecting airway remodeling and autophagy. *Respir Physiol Neurobiol*. 2022;306:103961.